

# Carrier-Phase-Based Initial Heading Alignment for Land Vehicular MEMS GNSS/INS Navigation System

Tisheng Zhang<sup>ID</sup>, Shan Liu<sup>ID</sup>, Qijin Chen<sup>ID</sup>, Xin Feng<sup>ID</sup>, and Xiaoji Niu<sup>ID</sup>

**Abstract**—For a micro-electromechanical system (MEMS)-based inertial navigation system (INS) and global navigation satellite system (GNSS) integrated system in land vehicular applications, rapid and accurate initial heading alignment is still a challenge. We propose an initial heading alignment method for MEMS INS using the GNSS carrier-phase measurement, based on the basic principle of trajectory similarity. The proposed method performs “trajectory matching” in the line-of-sight direction of satellites, where the angle is obtained by comparing the actual observed time-differenced carrier phase (TDCP) and INS-derived TDCP. Experimental results show that the initial heading could be determined accurate to  $0.65^\circ$  and  $1.68^\circ$  at a 95% confidence level within 5 s under open-sky conditions and in typical urban environments, respectively, using a typical MEMS inertial measurement unit (e.g., STIM300, Safran Sensing Technologies Norway) and high-quality GNSS receiver (NovAtel OEM6). The proposed method is also verified using a low-cost GNSS receiver and low-cost inertial measurement unit (IMU) chip under different environments. The proposed method performs better than existing approaches in terms of time efficiency and accuracy.

**Index Terms**—Carrier phase, global navigation satellite system (GNSS)/inertial navigation system (INS) integration, initial alignment, micro-electromechanical system (MEMS) inertial measurement unit (IMU), time-differenced carrier phase (TDCP).

## I. INTRODUCTION

**A**N inertial navigation system (INS) can navigate autonomously without relying on external information [1], which is based on dead reckoning (DR) navigation. The states of this system, including position, velocity, and attitude, must be initialized before the start of navigation. When compared to the identification of the initial attitude, the initialization of position and velocity is significantly easier because the initial position and velocity can be accurately

provided by a global navigation satellite system (GNSS). Traditionally, the initial alignment in a high-precision INS varies from that in a low-cost INS because of the distinct noise characteristics. In a high-quality inertial measurement unit (IMU), the traditional static alignment method performs attitude initialization by sensing the local gravity and rotation rate of Earth, which is called coarse alignment of the static alignment. Moreover, the pitch and roll of a micro-electromechanical system (MEMS) IMU can be determined using an accelerometer by sensing the gravity of Earth under the existence of a large local gravity. However, it is difficult to initialize the heading. Limited by technical and technological factors, the gyro bias instability is usually more than 15%h [2], [3]. Thus, the low performance of MEMS gyroscopes has resulted in challenges in heading initialization. Consequently, heading initialization has currently become an important and popular issue in the field of inertial navigation.

When analyzing dynamic scenes in vehicle navigation, auxiliary information must be provided for the heading alignment of the MEMS IMU. Common auxiliary information includes GNSS data [4], [5], odometer readings [6], [7], and Doppler velocity logs [8], [9], [10]. For example, the initial heading can also be determined using a pair of antennas mounted on the same vehicle [11]. When the INS is in motion, the vehicle heading can be determined from the GNSS velocity vector projected in the horizontal plane [11], [12] or determined from the GNSS trajectory [4], [13, p. 207]. These methods are straightforward, but the accuracy degrades when the vehicle turns and becomes unreliable at low speed.

For a more general solution, in recent years, two primary methods have been developed to implement a coarse alignment of the in-motion vehicle scene [14]: 1) Kalman filtering-based coarse alignment methods [3], [15], [16] and 2) optimization-based iterative method [7], [17], [18], [19], [20], [21]. The Kalman filtering-based method usually models the state errors accurately; therefore, accurate heading results can be obtained using this method. However, this method requires a long convergence time [22]. Han and Wang [3] proposed a two-stage Kalman filtering algorithm for low-cost INS, reporting  $0.3^\circ$  heading alignment accuracy in approximately 150 s. Wang *et al.* [14] proposed an adaptive unscented Kalman filter (KF) for the MEMS-based navigation of an unmanned aerial vehicle, whose root-mean-square error (RMSE) of the yaw angle was  $0.059^\circ$  for a convergence time

Manuscript received 16 May 2022; revised 19 August 2022; accepted 6 September 2022. Date of publication 22 September 2022; date of current version 5 October 2022. This work was supported in part by the National Key Research and Development Program of China under Grant 2020YFB0505803 and in part by the National Natural Science Foundation of China under Grant 41974024 and Grant 41904019. The Associate Editor coordinating the review process was Dr. Valentina Bianchi. (*Corresponding author: Qijin Chen.*)

Tisheng Zhang, Qijin Chen, and Xiaoji Niu are with the GNSS Research Center, Wuhan University, Wuhan 430072, China, and also with the Hubei Luoqia Laboratory, Wuhan 430079, China (e-mail: chenqijin@whu.edu.cn).

Shan Liu is with the GNSS Research Center, Wuhan University, Wuhan 430072, China.

Xin Feng is with the School of Geodesy and Geomatics, Wuhan University, Wuhan 430072, China.

Digital Object Identifier 10.1109/TIM.2022.3208646

1557-9662 © 2022 IEEE. Personal use is permitted, but republication/redistribution requires IEEE permission.  
See <https://www.ieee.org/publications/rights/index.html> for more information.

of 80 s. The optimization-based method is an innovative solution, which transforms the attitude alignment problem into a continuous attitude determination problem using infinite vector observation [23]. However, this method also requires a long convergence time [24]. Zhang *et al.* [2] proposed a velocity-based optimization-based alignment (OBA) method, reporting a  $4^\circ$  heading alignment accuracy within 60 s. Wei *et al.* [25] proposed a carrier Doppler-based initial alignment under low satellite visibility that required approximately 40 s to converge to  $1.57^\circ$  of average heading estimation error. Nowadays, several application scenarios require fast initialization capabilities for INSs equipped with MEMS IMUs [26]. The accuracy and the rate of initialization are significant. Therefore, a rapid and accurate initialization method is required.

A rapid and accurate INS alignment method was proposed in [12], specifically for tilted real-time kinematic (RTK) receivers. This method calculates the initial heading as the angle between the INS- and RTK-indicated increment vectors of the antenna phase center position in the horizontal direction based on the fact that the INS- and RTK-indicated trajectories are similar in shape but with a rotation of the heading error. This method is able to determine the IMU's initial heading angle accurately within only 2 s, thus resulting in a better performance in terms of both time efficiency and accuracy. However, this method requires the constraint of rigid body motion and is not suitable for land vehicular systems.

From the literature review, we notice that rapid and accurate heading alignment for land vehicular GNSS/INS integrated systems is still a challenge. We try to address this issue by proposing an initial heading alignment method using the time-differenced carrier phase (TDCP) that most GNSS receivers can generate [27]. This present work is inspired by the previous work [12], and the initial heading angle is determined based on the basic principle of trajectory similarity, but using the underlying measurement, i.e., delta carrier phase, instead of the GNSS positioning solution. The contribution of the present work is given as follows.

- 1) We use the TDCP for the first time as aiding to determine the initial INS heading based on the principle of trajectory similarity. The benefit of performing matching in the carrier-phase level is that the GNSS base station is no longer needed to enhance the accuracy. It performs well even when there are fewer than four satellites available. Thus, the proposed method is much more flexible and valid under different conditions.
- 2) The initial heading could be determined accurately at confidence level in only 5 s using typical MEMS IMU and GNSS receiver under open-sky conditions, which performs significantly better than the existing method in terms of time efficiency and accuracy. The proposed method is also verified using a low-cost GNSS receiver, IMU, and in challenging urban condition.

## II. METHODOLOGY

In this section, an overview of the approach is first presented. Then, we have described the proposed algorithm in detail. The implementation of the approach is presented finally.

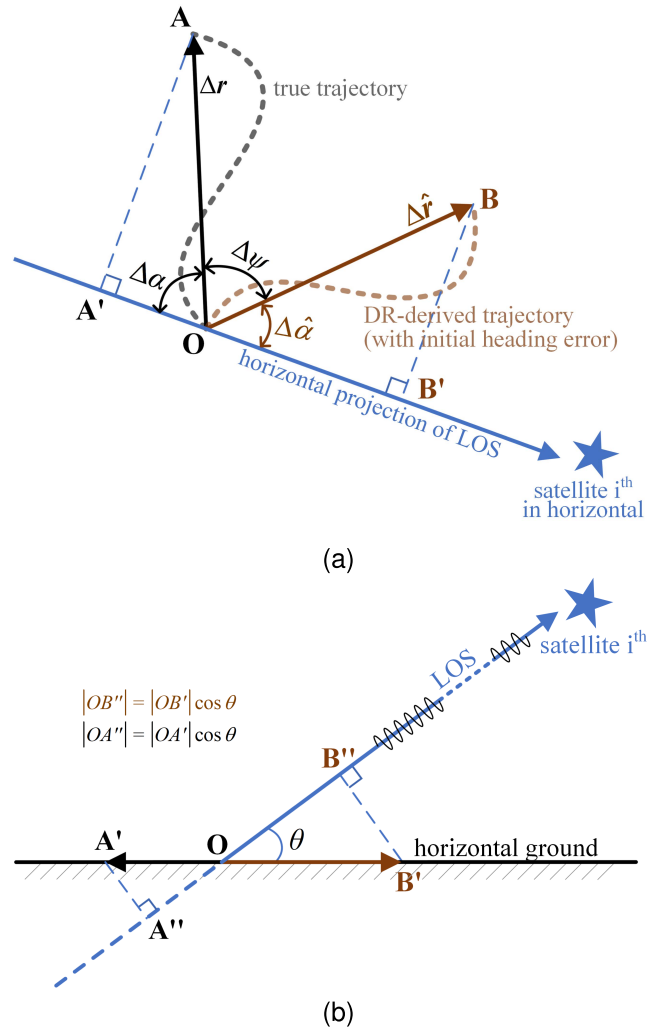


Fig. 1. Illustration of the initial heading alignment principle. (a) Top view of the true trajectory, DR-derived trajectory, and satellite. The true and DR-derived trajectories are similar in shape in the horizontal plane, but with a rotation of the heading error  $\Delta\psi$ . (b) Front view of the trajectories and carrier phase. Trajectories can be projected onto the LOS direction based on azimuth and elevation angle.

### A. Principle of the Proposed Method

Fig. 1 shows the principle of the initial heading alignment. In the alignment phase, the host vehicle moves on the ground, and synchronized raw IMU data and carrier-phase measurements of the GNSS receiver are transmitted to the alignment calculator. The GNSS receiver needs to continuously output the carrier phase of at least one satellite within the alignment period. The top of Fig. 1 shows the trajectory of the vehicle in the local horizontal plane. In this figure,  $\overrightarrow{OA}$  is the actual trajectory of the vehicle and  $\overrightarrow{OA}$  is the position increment vector, i.e., delta position vector denoted by  $\Delta r$ .  $\overrightarrow{OB}$  is the DR-derived trajectory obtained using IMU measurements, which is explained subsequently.  $\overrightarrow{OB}$  is the DR-derived position increment vector, i.e., delta position vector denoted by  $\Delta \hat{r}$ . Line  $A'OB'$  is the horizontal projection of the vector from the starting point of alignment to a given satellite, i.e., the line-of-sight (LOS) vector.

$A'$  and  $B'$  are the projection points of  $A$  and  $B$ , respectively, on the horizontal LOS. From this figure, we obtain

$$\Delta\alpha + \Delta\hat{\alpha} + \Delta\psi = 180^\circ \quad (1)$$

where  $\Delta\psi$  is the deviation of the arbitrarily given initial heading from the true heading, which is to be determined in the alignment. Equation (1) implies that as long as  $\Delta\alpha$  and  $\Delta\hat{\alpha}$  can be determined,  $\Delta\psi$  can be calculated, and the initial heading solution can be obtained.

In the bottom of Fig. 1, all the points are in the vertical plane passing through the LOS. From Fig. 1, we obtain

$$\frac{|OA''|}{|OB''|} = \frac{|OA'|\cos\theta}{|OB'|\cos\theta} = \frac{|OA|\cos\Delta\alpha}{|OB|\cos\Delta\hat{\alpha}}. \quad (2)$$

Consider that the lengths of trajectories  $\overrightarrow{OA}$  and  $\overrightarrow{OB}$  are equal, i.e.,  $|OA| = |OB|$ . From (2), we obtain

$$\frac{|OA''|}{|OB''|} = \frac{\cos\Delta\alpha}{\cos\Delta\hat{\alpha}}. \quad (3)$$

Thus, the procedure for determining  $\Delta\psi$ , i.e., initial heading alignment, is given as follows.

- 1) Compute the DR-indicated trajectory (refer to Section II-B) using travel distance and gyro-derived attitude by arbitrarily assigning an initial heading  $\psi_0$  of the INS (usually 0), where the given heading  $\psi_0$  has a deviation  $\Delta\psi$  from the actual initial heading. Thus, the determination of the initial heading means calculating  $\Delta\psi$ . We have proven in previous research [12] that the DR-derived and true trajectories are similar in shape but with a rotation of  $\Delta\psi$ , as shown in Fig. 1(a).
- 2) The azimuth of vector  $\overrightarrow{OB}$  is derived from the DR-derived positioning solution. The azimuth of the satellite can be calculated based on the satellite position and the initial position of the vehicle. Then, the angle between azimuth values of the trajectory vector and satellite  $\Delta\hat{\alpha}$  can be determined.
- 3)  $|OA''|$  and  $|OB''|$  are the lengths of the trajectory along the LOS direction.  $|OB''|$  can be derived from the DR positioning solution, and  $|OA''|$  can be measured from the carrier-phase measurement of the GNSS receiver, which is derived in detail in Section II-C. Thus,  $\Delta\alpha$  can be calculated according to (3).
- 4) According to (1), using  $\Delta\hat{\alpha}$  from step 2 and  $\Delta\alpha$  from step 3, the initial heading error  $\Delta\psi$  can be calculated.

## B. DR Position Computation

The vector  $\mathbf{r} = [B \ L \ H]^T$  describes the position of the vehicle in the geodetic coordinate system.  $B$ ,  $L$ , and  $H$  represent the geodetic latitude, longitude, and ellipsoidal height, respectively. The DR position can be updated by the following equations:

$$B_k = B_{k-1} + \frac{\Delta s_N}{R_M + H_{k-1}} \quad (4)$$

$$L_k = L_{k-1} + \frac{\Delta s_E}{(R_N + H_{k-1}) \cos B_{k-1}} \quad (5)$$

$$H_k = H_{k-1} - \Delta s_D \quad (6)$$

where  $R_M$  and  $R_N$  are the radii of curvature along the lines of constant longitude and latitude, respectively [28].  $\Delta \mathbf{s}^n = [\Delta s_N \ \Delta s_E \ \Delta s_D]^T$  represents the position incremental vector with components between times  $k$  and  $k-1$  in the north, east, and down directions in the north–east–down frame ( $n$ -frame).

The  $n$ -frame position incremental vector  $\Delta \mathbf{s}^n$  can be obtained from the position incremental vector  $\Delta \mathbf{s}^v(t_k)$  in the vehicle frame ( $v$ -frame, whose  $x$ -axis is consistent with the forward direction of the vehicle,  $z$ -axis points downward, and  $y$ -axis points outward) using the following equation:

$$\Delta \mathbf{s}^n(t_k) = \mathbf{C}_b^n(t_k) \mathbf{C}_v^b(t_k) \Delta \mathbf{s}^v(t_k) \quad (7)$$

where  $\mathbf{C}_b^n$  represents the rotation matrix that projects the vector from the  $b$ -frame (IMU body frame, whose axes are the same as those of the IMU) to the  $n$ -frame.  $\mathbf{C}_v^b$  represents the rotation matrix that projects the vector from the  $v$ -frame to the  $b$ -frame, which is determined by the IMU mounting angles. The position incremental vector  $\Delta \mathbf{s}^v(t_k)$  in the  $v$ -frame can be expressed as an integral of the velocity

$$\Delta \mathbf{s}^v(t_k) = \int_{t_{k-1}}^{t_k} \mathbf{v}^v(\tau) d\tau \quad (8)$$

where  $\mathbf{v}^v$  is the velocity vector in the  $v$ -frame, whose elements are zeros, except for the first one, and is expressed as  $\mathbf{v}^v = [v \ 0 \ 0]^T$ , which can be easily obtained from the GNSS position result or odometer output.

The attitude is updated with the direction cosine matrix based on the gyro output. The progress in update from time  $t_{k-1}$  to  $t_k$  is based on the direction cosine matrix chain rules [29], which are formulated as follows:

$$\mathbf{C}_b^n(t_k) = \mathbf{C}_{b(k)}^{n(k)} \approx \mathbf{C}_{b(k)}^n = \mathbf{C}_{b(k-1)}^n \mathbf{C}_{b(k)}^{b(k-1)} \quad (9)$$

$$\mathbf{C}_{b(k)}^{b(k-1)} = \mathbf{I}_3 + \sin \varphi_k (\mathbf{u}_k \times) + (1 - \cos \varphi_k) (\mathbf{u}_k \times)^2 \quad (10)$$

$$\varphi_k = \Delta \boldsymbol{\gamma}_k + \frac{1}{12} \Delta \boldsymbol{\gamma}_{k-1} \times \Delta \boldsymbol{\gamma}_k \quad (11)$$

where  $\mathbf{C}_b^n$  represents the rotation matrix that projects the vector from the  $b$ -frame to the  $n$ -frame,  $\varphi_k$  is the rotation vector, and  $\mathbf{u}_k$  is the unit rotation vector along  $\varphi_k$ .  $\Delta \boldsymbol{\gamma}_{k-1}$  and  $\Delta \boldsymbol{\gamma}_k$  are incremental angle measurements of the IMU.  $\mathbf{I}_3$  is a  $3 \times 3$  identity matrix.  $(\cdot \times)$  represents the cross-product (skew-symmetric) form of a given 3-D vector.

## C. Initial Heading Angle Computation

The carrier-phase measurement from the  $i$ th satellite is formulated as

$$\phi^i = \lambda^{-1} (d + \delta t_u - \delta t^{(s)} - I + T) + N + \varepsilon_\phi \quad (12)$$

where  $d$  represents the absolute LOS distance between the satellite and the receiver,  $\delta t^{(s)}$  and  $\delta t_u$  are the satellite and receiver clock errors, respectively,  $I$  and  $T$  are the ionosphere and troposphere propagation errors, respectively, and  $N$  is the carrier-phase integer ambiguity [30].

Since the proposed method is able to determine the initial heading angle in a short time, e.g., 5 s, in such short period of time  $\delta t^{(s)}$ ,  $I$  and  $T$  change slowly,  $N$  is fixed, and  $\delta t_u$  can be estimated by the receiver positioning. Therefore, TDCP  $\Delta \phi_{0,t}^i$

from the  $i$ th satellite between time 0 and  $t$  is primarily caused by the distance between the satellite and the receiver.

For simplicity, the TDCP can be expressed as

$$\begin{aligned}\Delta\phi_{0,t}^i &= \phi_t^i - \phi_0^i \approx \lambda^{-1}(d_t^i - d_0^i) \\ &= \lambda^{-1}(\mathbf{e}_t^i \cdot \mathbf{d}_t^i - \mathbf{e}_0^i \cdot \mathbf{d}_0^i) \\ &= \lambda^{-1}[\mathbf{e}_t^i \cdot (\mathbf{d}_0^i - \Delta\mathbf{r}_u - \Delta\mathbf{r}_s^i) - \mathbf{e}_0^i \cdot \mathbf{d}_0^i] \\ &= \lambda^{-1}[(\mathbf{e}_t^i - \mathbf{e}_0^i) \cdot \mathbf{d}_0^i + \mathbf{e}_t^i \cdot (-\Delta\mathbf{r}_s^i - \Delta\mathbf{r}_u)]\end{aligned}\quad (13)$$

where  $\mathbf{e}$  and  $\mathbf{d}$  are the unit vectors in the direction of satellite and the position vectors from the receiver to the satellite, respectively, with subscripts 0 and  $t$  indicating the epoch and superscript  $i$  indicating the satellite.  $\Delta\mathbf{r}$  is the position incremental vector between  $t$  and 0 epochs and subscripts  $u$  and  $s$  represent the user and satellite, respectively.

As the magnitude of  $\|\mathbf{e}_t^i - \mathbf{e}_0^i\|$  is small, even if the error of  $\mathbf{d}_0$  reaches 100 m, its influence on the distance can be neglected. Thus, (13) can be approximated as

$$\begin{aligned}\Delta\phi_{0,t}^i &\approx \lambda^{-1}[\mathbf{e}_t^i \cdot (-\Delta\mathbf{r}_s^i - \Delta\mathbf{r}_u)] \\ &= \lambda^{-1}(-\Delta d_s^i - \Delta d_u)\end{aligned}\quad (14)$$

where  $\Delta d_s^i$  and  $\Delta d_u$  are the  $i$ th satellite and user movements along the LOS direction, respectively. Therefore, the TDCP can be divided into two parts: the influence of satellite and receiver movements.

The distance of the receiver position increment along the LOS  $\Delta d_u$  can be expressed as

$$\Delta d_u = \mathbf{e}^i \cdot \Delta\mathbf{r}_u = \mathbf{e}^i (\mathbf{S}^{-1} \Delta\mathbf{r}_u^n). \quad (15)$$

$\Delta\mathbf{r}_u^n$  denotes the user position incremental vector expressed in the  $n$ -frame.  $\mathbf{S}$  is the coordinate transformation matrix that transforms the Cartesian coordinates to the  $n$ -frame

$$\mathbf{S} = \begin{bmatrix} -\sin B \cos L & -\sin B \sin L & \cos B \\ -\sin L & \cos L & 0 \\ -\cos B \cos L & -\cos B \sin L & -\sin B \end{bmatrix} \quad (16)$$

where  $B$  and  $L$  are the latitude and longitude of the origin of the  $n$ -frame, respectively, and  $\mathbf{S}$  is an orthogonal matrix that has determinant 1. Therefore, (15) can also be expressed as

$$\begin{aligned}\Delta d_u &= \mathbf{e}^i (\mathbf{S}^{-1} \Delta\mathbf{r}_u^n) = \frac{1}{d^i} \mathbf{d}^{e,i,T} \mathbf{S}^{-1} \Delta\mathbf{r}_u^n \\ &= \frac{1}{d^i} (\mathbf{S} \mathbf{d}^{e,i})^T \Delta\mathbf{r}_u^n = \frac{1}{d^i} \mathbf{d}^{n,i,T} \Delta\mathbf{r}_u^n\end{aligned}\quad (17)$$

where  $d^i$  denotes the absolute LOS distance between the GNSS receiver and the  $i$ th satellite.  $\mathbf{d}^{e,i} = [\Delta d_x^i \ \Delta d_y^i \ \Delta d_z^i]^T$  describes the vector from the GNSS receiver to the satellite in Cartesian coordinates, and it can be equivalently expressed as a vector  $\mathbf{d}^{n,i} = [\Delta d_N^i \ \Delta d_E^i \ -\Delta d_U^i]^T$  in the  $n$ -frame.

By retaining the horizontal coordinate components of the vector, we obtain

$$\begin{aligned}\Delta d_u &= \frac{1}{d^i} (\Delta d_N^i \Delta r_{u,N} + \Delta d_E^i \Delta r_{u,E} + \Delta d_U^i \Delta r_{u,U}) \\ &= \Delta d_{u,H} + \frac{1}{d^i} \Delta d_U^i \Delta r_{u,U}\end{aligned}\quad (18)$$

where  $\Delta d_{u,H}$  is the horizontal component of the user movement along the LOS direction and  $\Delta r_{u,N}$ ,  $\Delta r_{u,E}$ , and  $\Delta r_{u,U}$

are the north, east, and up components of the user position incremental vector  $\Delta\mathbf{r}_u^n$ , respectively.

The elevation angle  $\theta$  and azimuth  $\alpha_s$  of satellite  $i$  can be calculated based on the observation vector

$$\theta = \arcsin\left(\frac{\Delta d_U^i}{d^i}\right) \quad (19)$$

$$\alpha_s = \arctan\left(\frac{\Delta d_E^i}{\Delta d_N^i}\right). \quad (20)$$

Thus, (18) can be transformed as follows:

$$\begin{aligned}\Delta d_{u,H} &= \frac{1}{d^i} (\Delta d_E^i \Delta r_{u,E} + \Delta d_N^i \Delta r_{u,N}) \\ &= \frac{\sqrt{\Delta d_E^i{}^2 + \Delta d_N^i{}^2}}{d^i} \\ &\quad \times \left( \frac{\Delta d_E^i}{\sqrt{\Delta d_E^i{}^2 + \Delta d_N^i{}^2}} \frac{\Delta r_{u,E}}{\sqrt{\Delta r_{u,E}^2 + \Delta r_{u,N}^2}} \right. \\ &\quad \left. + \frac{\Delta d_N^i}{\sqrt{\Delta d_E^i{}^2 + \Delta d_N^i{}^2}} \frac{\Delta r_{u,N}}{\sqrt{\Delta r_{u,E}^2 + \Delta r_{u,N}^2}} \right) \\ &\quad \times \sqrt{\Delta r_{u,E}^2 + \Delta r_{u,N}^2} \\ &= \cos\theta (\cos\alpha_u \cos\alpha_s + \sin\alpha_u \sin\alpha_s) |\Delta\mathbf{r}_u^n| \\ &= |\Delta\mathbf{r}_u^n| \cos(\alpha_u - \alpha_s) \cos\theta.\end{aligned}\quad (21)$$

$\alpha_u$  denotes the azimuth of the user movement, which can be expressed as follows:

$$\alpha_u = \arctan\left(\frac{\Delta r_{u,E}}{\Delta r_{u,N}}\right). \quad (22)$$

After the above transformation, we can estimate TDCP based on the azimuth, elevation angle, and length of the vector  $\Delta\mathbf{r}_u^n$ . Substituting (21) into (14) and (18), we obtain

$$\begin{aligned}\Delta\phi_{0,t}^i &= \lambda^{-1} \left( -\Delta d_s^i - \Delta d_{u,H} - \frac{1}{d^i} \Delta d_U^i \Delta r_{u,U} \right) \\ &= \lambda^{-1} \left( -\Delta d_s^i - |\Delta\mathbf{r}_u^n| \cos(\alpha_u - \alpha_s) \cos\theta \right. \\ &\quad \left. - \frac{1}{d^i} \Delta d_U^i \Delta r_{u,U} \right).\end{aligned}\quad (23)$$

The increment in the carrier phase between the start and the end of the actual vehicle trajectory is called observed TDCP  $\Delta\tilde{\phi}$ . The increment in the carrier phase between the start and the end of the DR-derived trajectory is called DR-derived TDCP  $\Delta\hat{\phi}$ .

$\Delta\Phi$  represents the difference between the observed and DR-derived TDCP. According to our previous research [12], the vertical components of the true and DR-derived trajectories are identical. Therefore, the influence of satellite movement and the vertical component of user movement are canceled

out during this process

$$\begin{aligned}\Delta\Phi_{0,t} &= \Delta\tilde{\phi}^i - \Delta\hat{\phi}^i \\ &= \lambda^{-1} \left( -\Delta d_s^i - \Delta d_{u,H} - \frac{1}{d^i} \Delta d_U^i \Delta r_{u,U} \right) \\ &\quad - \lambda^{-1} \left( -\Delta d_s^i - \Delta \hat{d}_{u,H} - \frac{1}{\hat{d}^i} \Delta d_U^i \Delta \hat{r}_{u,U} \right) \\ &= \lambda^{-1} \left( |\Delta \mathbf{r}_u^n| \cos(\alpha_u - \alpha_s) \cos \theta \right. \\ &\quad \left. - |\Delta \hat{\mathbf{r}}_u^n| \cos(\hat{\alpha}_u - \alpha_s) \cos \theta \right). \quad (24)\end{aligned}$$

$\Delta \hat{\mathbf{r}}_u^n$  denotes the DR-derived trajectory.  $\Delta \mathbf{r}_u^n$  denotes the true trajectory.  $\hat{\alpha}_u$  is the azimuth of the DR-derived trajectory.

As discussed in our previous research [12], the DR-derived trajectory  $\Delta \hat{\mathbf{r}}_u^n(t) = [\Delta \hat{r}_{u,N}(t) \ \Delta \hat{r}_{u,E}(t)]^T$  is similar to the true trajectory  $\Delta \mathbf{r}_u^n(t) = [\Delta r_{u,N}(t) \ \Delta r_{u,E}(t)]^T$  in shape but has a constant rotation because of the occurrence of the initial heading bias  $\Delta\psi$

$$\Delta \hat{\mathbf{r}}_u^n(t) = \mathbf{C}_n^{\hat{n}} \Delta \mathbf{r}_u^n(t) \quad (25)$$

where  $\mathbf{C}_n^{\hat{n}}$  is the directional cosine matrix that transforms the real  $n$ -frame to the misaligned  $\hat{n}$ -frame. The errors in the misaligned  $\hat{n}$ -frame stem from the initial heading errors. Moreover, the matrix  $\mathbf{C}_n^{\hat{n}}$  can be approximated according to the conversion from Euler angles to the attitude matrix [31] as follows:

$$\mathbf{C}_n^{\hat{n}} = \begin{bmatrix} \cos \Delta\psi & -\sin \Delta\psi \\ \sin \Delta\psi & \cos \Delta\psi \end{bmatrix}. \quad (26)$$

Therefore, the initial heading bias  $\Delta\psi$  can be described based on the azimuth of the DR-derived and true trajectories

$$\Delta\psi = \hat{\alpha}_u - \alpha_u. \quad (27)$$

According to our previous research [12],  $|\Delta \mathbf{r}_u^n|$  is equal to  $|\Delta \hat{\mathbf{r}}_u^n|$ . Thus, (24) can be expressed as

$$\cos(\alpha_u - \alpha_s) = \frac{\Delta\Phi_{0,t} \lambda}{|\Delta \mathbf{r}_u^n| \cos \theta} + \cos(\hat{\alpha}_u - \alpha_s). \quad (28)$$

The azimuth of the true trajectory  $\alpha_u$  can be derived from (28). Since the cosine value of both  $(\alpha_u - \alpha_s)$  and  $(\alpha_s - \alpha_u)$  is the same, there are two possible solutions of  $\alpha_u$  to (28). However, only one of them is what we need. This ambiguity can be eliminated in the following approaches.

- 1) Solving this equation with aid of the coarse positioning solution from single-point positioning (SPP), since we can roughly compute the azimuth from the delta position vector, as  $\psi = \arctan(\Delta r_E / \Delta r_N)$ , where  $\Delta r_E$  and  $\Delta r_N$  are the position changes in east and north direction, respectively. Then, we are able to choose the correct solution that is close to the computed  $\psi$ .
- 2) The principle of determining the correct solution using measurements from multiple satellites is given as follows: since each satellite has a solution close to the true heading, by comparing the solutions from multiple different satellites, the correct solution can be determined. In addition, by choosing the solution with the shortest distance to the GNSS-indicated result, we can also determine the solution.

#### D. Practical Implementation

To obtain the calculated carrier phase of the point  $\hat{\mathbf{r}} = [B \ L \ H]^T$  on the DR-derived trajectory, the position vector  $\hat{\mathbf{r}}$  in the geodetic curvilinear coordinate must be converted to the point  $\mathbf{p} = [x \ y \ z]^T$  in the Cartesian coordinate. This conversion can be completed by the following equations:

$$x = (a + H) \cos B \cos L \quad (29)$$

$$y = (a + H) \cos B \sin L \quad (30)$$

$$z = [a(1 - \epsilon^2) + H] \sin B. \quad (31)$$

Here,  $a$  is the transverse radius of curvature of Earth and  $\epsilon$  is the eccentricity of the ellipsoid.

The satellite positions  $\mathbf{p}_S^i = [x^i \ y^i \ z^i]^T$  can be derived from an ephemeris. The distance  $d^i$  from the point on the ground to the satellite with pseudorandom noise (PRN)  $i$  is calculated as follows:

$$d_{DR}^i = \sqrt{(x - x^i)^2 + (y - y^i)^2 + (z - z^i)^2}. \quad (32)$$

The TDCP of the DR-derived trajectory can be calculated as

$$\Delta \hat{\phi}_{0,t}^i = \lambda^{-1} (d_{DR}^i(t) - d_{DR}^i(0)). \quad (33)$$

The TDCP of the true trajectory is derived from the carrier-phase observation measured by the GNSS receiver as follows:

$$\Delta \tilde{\phi}_{0,t}^i = \tilde{\phi}_t - \tilde{\phi}_0 \quad (34)$$

where  $\tilde{\phi}$  denotes the observations of the GNSS receiver.

The implementation process is presented in Algorithm 1.

---

#### Algorithm 1 Initial Heading Alignment Using Carrier-Phase Measurement

---

INPUT:  $\Delta s_k^v$ ,  $\mathbf{r}_0$ ,  $\Delta\theta_{k-1}$ ,  $\Delta\theta_k$ ,  $\tilde{\phi}_t$ ,  $\tilde{\phi}_0$ .

CALCULATE DR-DERIVED TRAJECTORY

1. Assign an arbitrary initial heading and form the initial attitude matrix  $\mathbf{C}_b^n(0)$ .
2. Update the attitude matrix  $\mathbf{C}_b^n(t_k)$  with gyro-derived measurements  $\Delta\theta_{k-1}$  and  $\Delta\theta_k$  using (9-11).
3. Update the DR-derived position  $\mathbf{r}_k$  with initial position value  $\mathbf{r}_0$  and travel distance  $\Delta s_k^v$  using (4-6).
4. Repeat step 2 and 3 until a DR-derived trajectory of specific duration is generated.

CALCULATE TIME-DIFFERENCED CARRIER PHASE

5. Compute the TDCP of the DR-derived trajectory  $\Delta \hat{\phi}_{0,t}^i$  using (29-33).
6. Compute the observed TDCP  $\Delta \tilde{\phi}_{0,t}^i$  with carrier phase observations  $\tilde{\phi}_t$  and  $\tilde{\phi}_0$  using (34).

CALCULATE INITIAL HEADING ANGLE

7. Compute the azimuth  $\hat{\alpha}_u$  of the DR-derived trajectory using (22).
8. Compute the azimuth  $\alpha_u$  of the true vehicle trajectory using (28).
9. Compute the initial heading bias  $\Delta\psi$  using (27).

OUTPUT:  $\Delta\psi$ .

---

### III. ERROR ANALYSIS

According to (27), the initial heading angle  $\Delta\psi$  is calculated based on the difference between the azimuth of the DR-derived trajectory  $\hat{\alpha}_u$  and the true trajectory  $\alpha_u$ . Thus, the error in the heading angle comprises the errors of the DR-derived trajectory azimuth and true trajectory azimuth, which can be computed as follows:

$$\delta\hat{\alpha}_u = \frac{\delta\Delta\hat{r}_{u,H}^n}{|\Delta\mathbf{r}_u^n|} \quad (35)$$

$$\delta\alpha_u = \arccos\left(\frac{\delta\Delta\tilde{\phi}_{0,t}\lambda}{|\Delta\mathbf{r}_u^n|\cos\theta}\right) \quad (36)$$

where  $\delta\hat{\alpha}_u$  denotes the error of the DR-derived trajectory azimuth and  $\delta\alpha_u$  denotes the error of true trajectory azimuth.  $\delta\Delta\hat{r}_{u,H}^n$  is the horizontal error component of the DR-derived trajectory  $\Delta\hat{r}_u^n$ .  $|\Delta\mathbf{r}_u^n|$  is the length of the movement vector, and we can observe that the heading alignment error is inversely proportional to the length of the travel trajectory.  $\delta\Delta\tilde{\phi}_{0,t}$  represents the error in the observed TDCP.  $\lambda$  is the wavelength of the carrier phase.  $\theta$  is the elevation angle of the satellite. Therefore, the initial heading estimation accuracy is influenced by the error in the DR-derived trajectory and the GNSS measurement. The equation above implies that for a given travel length, i.e.,  $|\Delta\mathbf{r}_u^n|$ , the more accurate the DR-derived trajectory is, the more accurate the initial heading should be. In contrast, the alignment error is inversely proportional to the trajectory length.

In practice, several GNSS observations with different PRNs can be measured in each epoch, which is identical to the number of initial heading angles that can be calculated during the process. Integration of these results improves the accuracy. Therefore, an analysis of the accuracy of different satellites is significant. According to (28), the angle between the azimuth of the satellite and the trajectory ( $\alpha_u - \alpha_s$ ) is a factor that influences accuracy. The number of satellites also influences the integration accuracy.

Subsequently, we will analyze the four main factors affecting alignment, in order of importance. The four factors are carrier-phase measurement error, satellite geometry, DR error, and the number of satellites.

#### A. Impacts of Carrier-Phase Measurement Error

TDCP is used to denote the true trajectory and is calculated by subtracting the carrier-phase observations between two epochs. From the carrier-phase observation equation (12), we can derive the equation of TDCP, which is expressed as

$$\Delta\phi = \lambda^{-1}(\Delta d + \Delta\delta t_u - \Delta\delta t^{(s)} - \Delta I + \Delta T) + \Delta N + \Delta\varepsilon_\phi \quad (37)$$

where  $\Delta\phi$  is the TDCP of a satellite between two measuring epochs.  $\lambda$  is the wavelength of the carrier phase.  $\Delta d$  denotes the increment of the absolute LOS distance between the satellite and the receiver.  $\Delta\delta t_u$  and  $\Delta\delta t^{(s)}$  represent the increments in the receiver and satellite clock errors, respectively.  $\Delta I$  and  $\Delta T$  denote the increments in the ionosphere and troposphere propagation errors, respectively.

Atmospheric propagation error in the TDCP can be neglected [32]. It should be noted that  $\Delta d$ ,  $\Delta\delta t_u$ ,  $\Delta\delta t^{(s)}$ ,  $\Delta I$ , and  $\Delta T$  represent distance measurement and are expressed in units of meters.  $\Delta N$  is the increment in the integer carrier-cycle ambiguity. Assuming that the ambiguity does not change during a short period,  $\Delta N$  can be removed.  $\Delta\varepsilon_\phi$  represents the unknown error during the measurement. In the carrier-phase observations, the precision of  $\varepsilon_\phi$  is in the millimeter scale, which implies that  $\Delta\varepsilon_\phi$  is relatively small and can be safely ignored [30].

Satellites contain highly stable atomic clocks that control all onboard timing operations. According to [33], the rate of change in the satellite clock error is typically 1–2 mm/s over short intervals. This implies that the TDCP error introduced by the satellite clock error is approximately 0.5–1.0 mm as long as the alignment is finished in a short time, for example, 5 s. The reason why we choose a period of 5 s is explained in IV-B. Therefore, the satellite clock error can be safely ignored.

Generally, receivers contain quartz clocks, which exhibit worse performance than the atomic clock. Quartz clocks not only have a large clock bias but also change quickly. It is difficult to model this error due to the irregularity of its changes. The receiver clock results in carrier-phase measurement errors that are uncorrelated over space and time, which implies that the receiver clock drift is the primary error in TDCP.

The receiver clock drift or accuracy varies for different types of receivers. The high-quality geodetic receivers typically estimate and compensate for the receiver clock drift every second, while the low-cost receivers do not. Thus,  $\Delta\delta t_u$  of high-quality receiver is small. For a low-cost GNSS receiver, the receiver clock drift may be significant and must be considered in the alignment. Fortunately, it can be estimated and compensated to an acceptable accuracy level from GNSS positioning processing and the residual  $\Delta\delta t_u$  after compensation is also relatively small. The residual clock drift of the high-quality receiver does not exceed 0.1 m/s [34], which implies that, in the worst case,  $\delta\Delta\tilde{\phi}_{0,t}\lambda = 0.5$  m, if the alignment period is set to 5 s. In the most general case, we assume that  $|\Delta\mathbf{r}_u^n| = 70$  m and the satellite elevation  $\theta = 45^\circ$ . Then, the error of the cosine value is  $0.5/(70 \text{ m} \times \cos 45^\circ) \approx 0.01$ . Assuming that the angle between the azimuth of the satellite and trajectory ( $\alpha_u - \alpha_s$ ) ranges from  $30^\circ$  to  $150^\circ$ , the error in the carrier phase indicated that the azimuth value  $\delta\alpha_u$  ranged from  $0.57^\circ$  to  $1.127^\circ$ .

The maximum multipath error of the carrier-phase measurement is  $0.25\lambda$  [35]. According to (36), the multipath leads to a maximum  $0.1^\circ$  heading error supposing that  $|\Delta\mathbf{r}_u^n| = 70$  m.

#### B. Impacts of Satellite Geometry

Satellite geometry is determined with the azimuth  $\alpha_s$  and elevation angle  $\theta$  of the satellite, which will be analyzed subsequently.

Solving the azimuth of the user trajectory  $\alpha_u$  using (28) is a key step for calculating the initial heading angle, where inverse trigonometric functions must be solved. Errors on the right-hand side of (28) do not directly affect the azimuth of the trajectory  $\alpha_u$ ; however, they affect the cosine of ( $\alpha_u - \alpha_s$ ). Therefore, the same magnitude of errors on the right-hand side of the equation will have a different impact on ( $\alpha_u - \alpha_s$ ) due

to the difference in the value of  $(\alpha_u - \alpha_s)$  itself. According to the properties of cosine functions, the corresponding delta angle caused by the same delta cosine value is large when the angle is approximately  $0^\circ$  and small when the angle is approximately  $90^\circ$ . Let us consider the aforementioned receiver clock error as an example; the unstable receiver clock brings an uncertainty of 0.01 to the cosine, which will lead to an uncertainty of  $0.57^\circ$  in  $(\alpha_u - \alpha_s)$  when  $(\alpha_u - \alpha_s) = 90^\circ$  and  $8.11^\circ$  in  $(\alpha_u - \alpha_s)$  when  $(\alpha_u - \alpha_s) = 0^\circ$ . This implies that the angle between the azimuth of the user trajectory and satellite has a significant effect on the initial heading. When the azimuth of the satellite is perpendicular to the azimuth of the user movement, the initialization process will exhibit a better performance. However, when the vehicle moves toward the satellite, the accuracy of the heading angle will drop rapidly.

Another factor is the elevation of the satellite. Equation (36) clearly shows that the heading error is inversely proportional to the cosine of elevation. Under the condition of identical TDCP errors, when the elevation of the satellite  $\theta$  is close to  $\pi/2$ , which implies that the satellite is almost directly above the receiver, the TDCP error will be amplified and the accuracy of the alignment will decrease significantly. However, when the elevation is close to 0, the accuracy is not improved because the error in the carrier-phase observations is larger. Therefore, it is necessary to screen out the satellites with low and high elevations.

### C. Impacts of DR-Indicated Error

The DR positioning error is induced by gyro-derived attitude and travel distance. Travel distance, which is measured using the odometer or GNSS data, can be measured accurately. Therefore, gyro-derived attitude is a major error source, which can be divided into the following four parts.

- 1) *Random Noise*: Angular random walk (ARW) is often used to represent random noise. The low-cost IMU, i.e., ICM20602, which is used in our field tests, has the ARW of  $0.24^\circ/h^{1/2}$ . According to [13, p. 207], the standard deviation of ensuring attitude error is  $\delta\psi = ARW(t)^{1/2} = 0.24 \times (5/3600)^{1/2} = 0.009^\circ$  after 5 s of integration, which is negligibly small.
- 2) *Fixed Gyro Bias*: Gyro bias can be modeled as a random constant because the gyro bias changes slowly in the short alignment period of time, e.g., 5 s. Fixed gyro bias leads to an approximately linear attitude drift over short periods of time. This can be initially estimated by averaging the gyro measurements, while the IMU remains stationary in practice. Since there exists Earth rotation rate, which is about  $15^\circ/h$ , and the gyro noise, which is about  $7.2^\circ/h$  when ARW is  $0.12^\circ/h^{1/2}$ , an error of  $(15^2 + 7.2^2)^{1/2} = 16.6^\circ/h$  will lead to the estimated bias. The attitude drift induced by the gyro bias does not exceed  $16.6^\circ/h \times 5 \text{ s} = 0.02^\circ$  within 5 s, which can be ignored [12].
- 3) *Cross-Coupling Error*: For a land vehicle, the changes in pitch and roll are usually small; therefore, the effect of cross-coupling can be ignored.

- 4) *Scale Factor Error*: The scale factor errors cause heading errors when vehicles turn around. Typical MEMS IMUs usually have a scale factor of 0.5% [12]. If the vehicle turns at an angle of  $90^\circ$ , the gyro-derived attitude error would be  $90^\circ \times 0.5\% = 0.45^\circ$ . This attitude error will eventually lead to an error in the azimuth of the DR-derived trajectory, which is half of the gyro-derived attitude error in the worst case when vehicles turn around, i.e.,  $0.45^\circ \times 0.5\% = 0.225^\circ$ .

Therefore, from the above analysis, the DR error is primarily induced by the gyro scale factor error, which can result in a maximum of  $0.225^\circ$  of azimuth error.

### D. Impacts of Satellites Number on Alignment

The error caused by the receiver clock drift exhibits a different magnitude and direction of impact on the initial heading. Let us consider a simple situation, in which two satellites with the same elevation but different azimuth values are symmetrical with respect to the vector of the increment in the true vehicle position. The common-mode errors in the TDCP, such as receiver clock errors, will lead to initial heading errors that are identical in magnitude but opposing in direction. Therefore, by averaging the results using these two satellites, the error caused by the receiver clock drift is eliminated. In practice, such ideal pairs of satellites generally do not exist. However, if multiple satellites located in different directions can be observed, averaging the heading solutions obtained from these different satellites can significantly eliminate the heading errors caused by common-mode errors in the observations. As the number of available satellites increases, the proposed algorithm becomes more robust since we have sufficient observations allowing us to detect outliers in the measurements.

Full determination of the impacts of the number and geometry of available satellites through a theoretical approach is complex. Here, we give two examples by assuming that there are four satellites available to illustrate the best and worst cases.

- 1) *Best Case*: Four satellites are symmetrically distributed with respect to the direction of vehicle trajectory, and assume the measurement of which have the same carrier-phase error. The heading error of two pairs of these four satellites is identical in magnitude but opposing in direction. By averaging the estimated heading results, a heading error will reduce to zero.
- 2) *Worst Case*: The four satellites are located in the same direction of vehicle trajectory. Suppose that the error of carrier-phase observations and DR are both in the worst case, which assumes  $\delta\vec{\phi}_{0,t}\lambda = 0.5 \text{ m}$  and  $\delta\alpha_{DR} = 0.225^\circ$ . Then, the heading error of one satellite is  $8.11^\circ$ , and averaging does not have any improvement in alignment accuracy.

## IV. EXPERIMENTS AND RESULTS

The proposed alignment method was evaluated and verified using two different types of IMUs and two different types of



Fig. 2. Photographs of the field test equipment.

GNSS receivers, in both open-sky areas and challenging urban environments.

#### A. Experiment Description

Experiments were conducted using a civilian land vehicle in Wuhan, China. Fig. 2 shows the photograph of the experimental setup. In these tests, a high-quality GNSS receiver (OEM6, NovAtel) and a low-cost GNSS receiver (M8P module, u-blox) were used to collect the carrier-phase observations. Two MEMS IMUs with different grades, i.e., STIM300 (Safran Sensing Technologies Norway) and ICM-20602 (InvenSense, TDK Group), were used to collect the raw IMU data. STIM300 is a quasi-tactical grade MEMS IMU. ICM-20602, a low-cost MEMS IMU chip, is integrated in an INS-Probe, which is a self-developed MEMS GNSS/INS integrated system [36]. STIM300 and ICM20602 recorded raw IMU data at a sampling rate of 125 and 50 Hz, respectively. A high-precision navigation grade position and orientation system, named POS-A15, is used as a reference system, which is able to provide heading reference accurate to  $0.01^\circ$ . The antenna is a high-quality GNSS antenna (HX-CSX601A, Harxon). The primary specifications of the equipment used in this experiment are listed as follows.

- 1) *GNSS Receiver*: NovAtel OEM6, a high-quality GNSS receiver, and u-blox M8P module, a low-cost GNSS receiver module. They are used to verify the proposed method using different types of receivers.
- 2) *MEMS IMU*: STIM300, a high-performance MEMS IMU; ICM-20602, a low-cost MEMS IMU chip. They are used to compare the performance of the method when using IMUs with different accuracy. Table I lists the parameters of these two IMU.
- 3) *Independent reference system*: POS-A15, which is capable of providing the reference attitude with an accuracy of  $0.01^\circ$ .

Fig. 3 shows the test path under open-sky conditions, which contains sufficient straight-line and curved segments to allow the vehicle to experience different dynamics. Similar tests

TABLE I  
SPECIFICATIONS OF IMUS

Parameter	STIM300	ICM-20602
Gyroscope angular random walk ( $^\circ/\sqrt{h}$ )	0.2	0.24
Gyroscope bias instability ( $^\circ/h$ )	0.5	10
Accelerometer velocity random walk ( $m/s/\sqrt{h}$ )	0.06	0.04
Accelerometer bias instability (mGal)	50	25

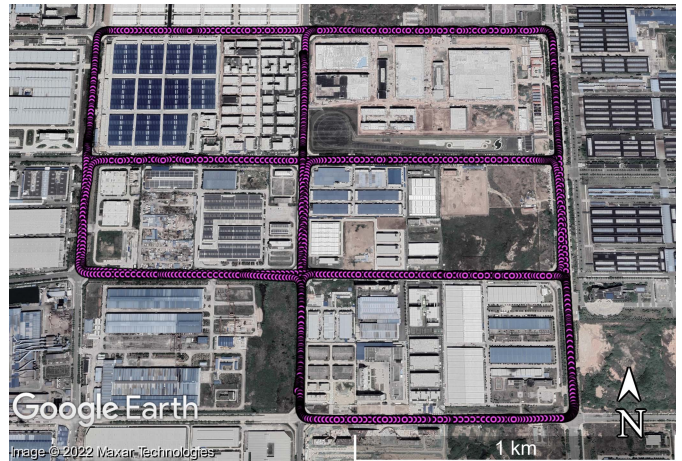


Fig. 3. Field test route under open-sky condition (from Google Earth).

were repeated in urban scenario in Wuhan dense city areas, with the same equipment to verify the proposed method under different hardware configurations and under different environments.

#### B. Data Processing

We first take the experiments under open-sky conditions as an example to analyze the results in detail and then repeated the analysis procedure for other tests. The experiment under open sky lasted about 50 min and can support 1506 alignment samples with a 5-s alignment period. The choice of 5 s will be explained later. The trajectory length of each alignment sample was greater than 5 m. Each alignment sample was processed independently with the data extracted from the raw IMU data, single-frequency L1 carrier-phase observations at 1 Hz of Global Positioning System (GPS) and BeiDou Navigation Satellite System (BDS), and GNSS position solution at 1 Hz. The alignment period was set to 5 s, considering the speed and accuracy of the alignment. It should be noted that, although we validated the algorithm by processing the collected data, the proposed method can also be implemented in a real-time case. Each sequence of carrier-phase observations in an alignment sample can deduce an initial heading result. We used the average of all observable satellite results as the result of the alignment samples. The data processing steps are described as follows.

- 1) Extract synchronized raw IMU data, GNSS positioning data, and carrier-phase observations for a period of 5 s from the alignment start time. Choose the satellites with sequence observations.
- 2) Process the alignment sample of each available satellite from step 1 using Algorithm 1. Calculate the average value of the initial heading results of each satellite as the heading alignment of this sample.
- 3) Determine the alignment error by comparing the calculated heading results with the reference heading. The calculated heading results are obtained from step 2 and the reference heading result is provided by the reference system.
- 4) Move the alignment start time to the next epoch. Repeat steps 1–3 to calculate the next heading and determine the next alignment error.
- 5) Repeat steps 1–4 to calculate the heading errors of the next dataset.

It should be noted that the period of 5 s in step 1 is an empirical value, which is chosen by considering both the time efficiency and accuracy of the proposed alignment method: 1) it is desirable to finish the alignment procedure in as short time as possible and 2) favorable accuracy should be achieved within this chosen period. If the alignment period is too short, for example, 1 s, the vehicle movement along the LOS direction may be not long enough, which leads to a larger alignment error. In contrast, a longer period means that the DR navigator works standalone in longer time, which would lead to a larger error in the DR-derived trajectory and result in an accuracy degradation in alignment. Therefore, 5 s is chosen in a compromised approach considering both the errors in both DR-derived trajectory and the movement length.

*C. Results*

The top of Fig. 4 shows the heading errors of each independent sample using measurements from STIM300 and the high-quality GNSS receiver under open-sky conditions. The heading error of each independent sample is obtained by averaging the results of all satellites available at that moment, i.e., totally 9–23 satellites. Fig. 5 plots the cumulative distribution of the alignment errors in the top of Fig. 4, from which we can read that initial heading could be determined accurately to 0.65° at a 95% confidence level within only 5 s. In a previous study, Zhang *et al.* [2] proposed the velocity-based OBA method to converge the initial heading alignment accuracy to 4° in 60 s. Huang *et al.* [5] showed in his work that the best performance of the previous method was a 2° heading alignment accuracy in approximately 75–100 s. Wei *et al.* [25] proposed the carrier Doppler-based initial alignment method that required approximately 40 s to converge, and the average heading error after convergence was 1.65°. Compared with previous research, the proposed method performs better in terms of accuracy and time efficiency.

In the top of Fig. 4, we notice that the heading errors of certain samples are significantly larger than others, such as samples 120, 220, and 400. By comparing the heading errors with the motion of the vehicle, we find that these larger errors

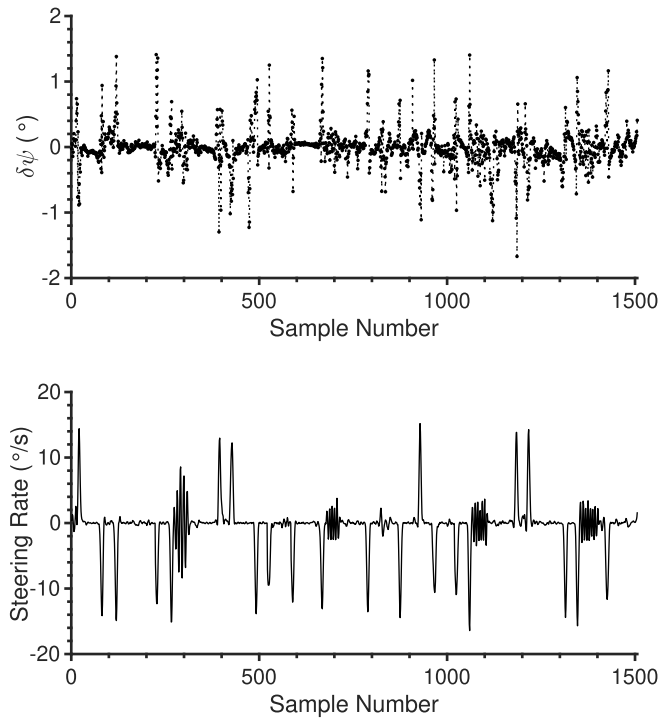


Fig. 4. Initial heading alignment errors (top) and the correlation with vehicle steering rate (bottom) using STIM300 and NovAtel OEM6 receiver under open-sky conditions.

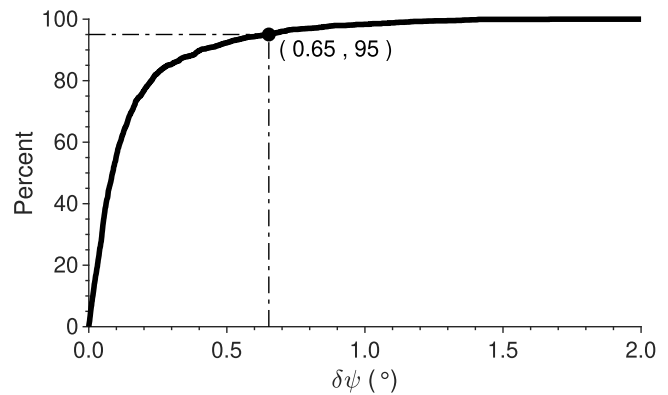


Fig. 5. CDF plot of initial heading alignment errors using STIM300 and NovAtel OEM6 receiver under open-sky condition.

occurred when the vehicle turned around. To visualize this phenomenon, we plot the vehicle steering rate together with the alignment error in Fig. 4. It shows that the initial heading errors are highly correlated with the turning motion of the vehicle.

In the top of Fig. 4, we also notice that the initial heading errors of certain samples are larger than others; however, there was no significant turning motion of the vehicle, such as in samples 836 and 1121. This occurred because the angle between the azimuth of the satellite  $\alpha_S$  and user movement  $\alpha_U$  has an impact on the accuracy of the initial heading. Fig. 6 shows the correlation of the heading error  $\delta\psi$  and the angle between two azimuths. The results of six satellites

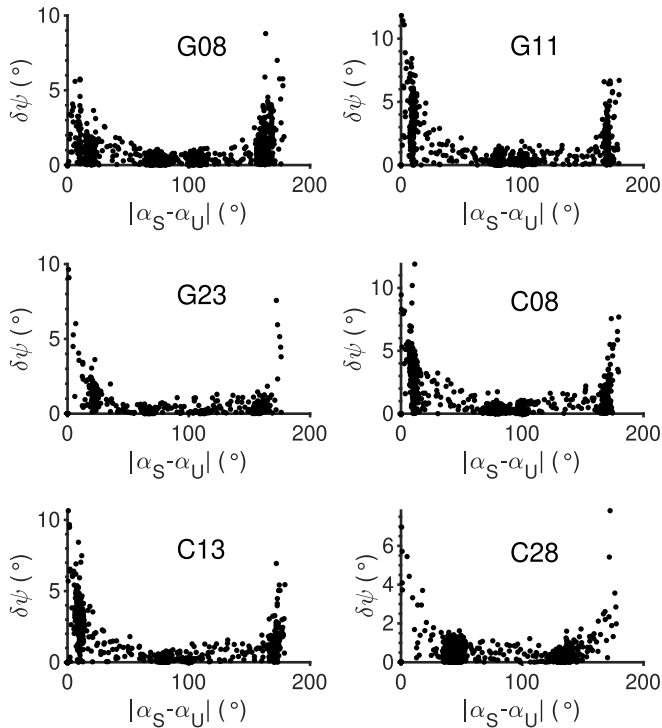


Fig. 6. Correlation of the initial heading errors  $\delta\psi$  and the angle between the azimuth of the satellite  $\alpha_S$  and user movement  $\alpha_U$ . *G* refers to GPS and *C* denotes BDS.

were chosen to illustrate this issue. They reveal that when  $|\alpha_S - \alpha_U|$  approaches  $0^\circ$  or  $180^\circ$ , the maximum value of the heading errors is marginally larger. Conversely, when the delta azimuth is approximately  $90^\circ$ , the maximum value of the heading errors is less. This implies that, when the azimuth of the satellite is perpendicular to that of user movement, this alignment will achieve the best performance. The maximum value of the heading error increases at approximately  $30^\circ$  and  $150^\circ$ , and the heading errors in the azimuth range of  $30^\circ$ – $150^\circ$  exhibited a similar performance in terms of maximum error. Thus, we can conclude that the initial heading is more feasible when the angle between the azimuth of the satellite  $\alpha_s$  and the user movement  $\alpha_u$  ranges from  $30^\circ$  to  $150^\circ$ .

To verify the proposed method, we plot the cumulative distribution function (cdf) curves of the alignment errors using different individual satellites in Fig. 7; 22 satellites with delta azimuth ranging from  $30^\circ$  to  $150^\circ$  were compared. A comparison shows that this heading alignment accuracy exhibits a good consistency by using different satellites. The accuracy of the initial heading calculated by an individual satellite alone ranges from  $0.7^\circ$  to  $1.47^\circ$  at a 95% confidence level. Moreover, 18 satellites have a heading accuracy of less than  $1.0^\circ$  at a 95% confidence level. When comparing the heading errors calculated based on an individual satellite with the average heading errors, as shown in Fig. 7, we notice that initial heading alignment accuracy improves to some extent.

The proposed method was also verified using a low-cost IMU chip, i.e., ICM20602, as shown in Fig. 8. Similar to Fig. 4, the alignment errors are also the averages of all

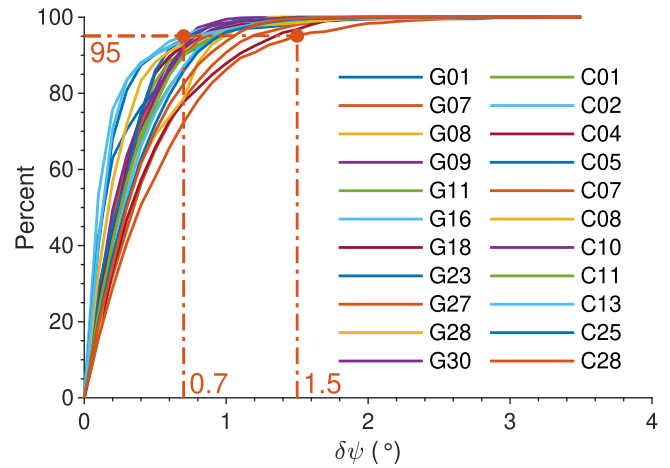


Fig. 7. CDF of the initial heading alignment errors using measurement of different individual satellites (NovAtel OEM6, under open-sky condition).

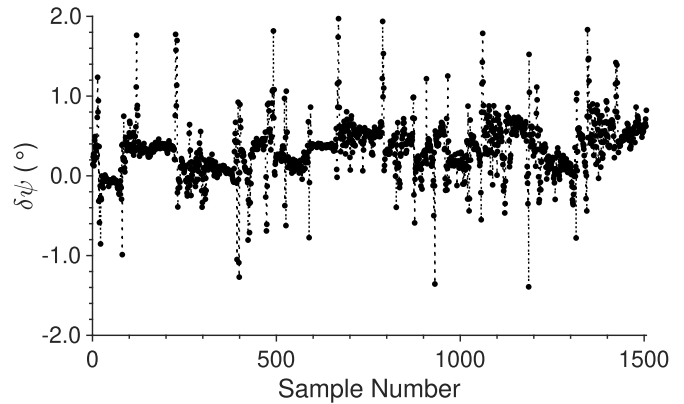


Fig. 8. Initial heading alignment errors using ICM-20602 and NovAtel OEM6 receiver under open-sky condition.

observable satellites, and the samples include the vehicle turning-around scenes. This result shows that the proposed method can achieve  $0.85^\circ$  at a 95% confidence level within 5 s using a low-cost IMU chip and high-quality GNSS receiver under open-sky conditions. Compared with the result using STIM300, the alignment accuracy using a low-cost IMU chip under open sky has no significant degradation.

To verify the application of the proposed method when using a low-cost GNSS receiver module, Fig. 9 shows the initial heading errors of each independent sample based on u-blox M8P. Since the low-cost GNSS receivers do not estimate and compensate for the receiver clock drift when generating the observations, the accumulation of receiver clock drift obtained from the SPP solution was used to compensate for the observations. The results shown in Fig. 9 are the averages of all observable satellites. The alignment samples include turning-around scenes. The results show that the proposed method can achieve  $0.93^\circ$  at a 95% confidence level within 5 s using high-performance MEMS IMU and low-cost GNSS receiver module under open-sky conditions. Compared with the result using a high-quality GNSS receiver, the alignment accuracy using a low-cost receiver under open sky has no obvious degradation.

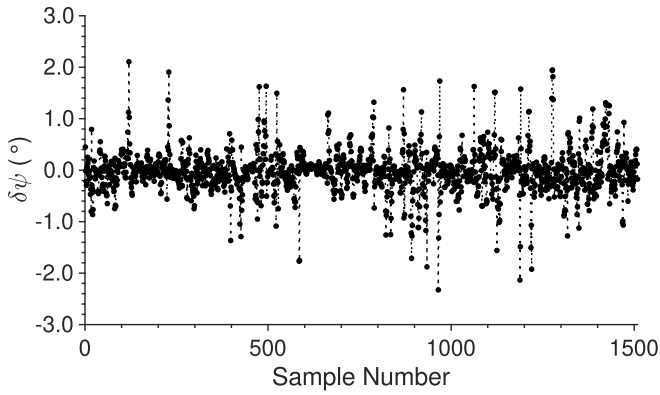


Fig. 9. Initial heading alignment errors using STIM300 and u-blox M8P GNSS receiver module under open-sky condition.

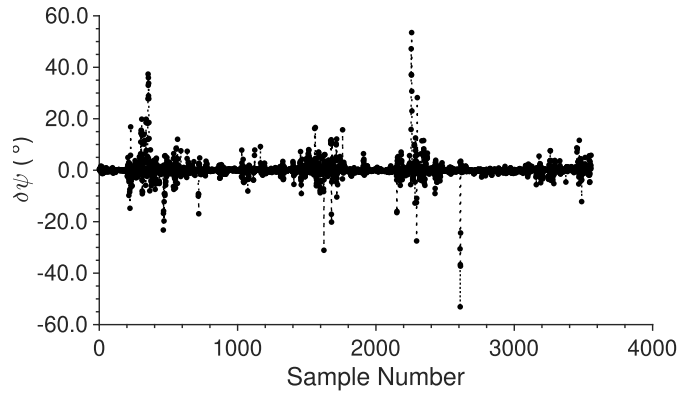


Fig. 11. Initial heading alignment errors by using STIM300 and u-blox M8P GNSS receiver module in typical urban environments.

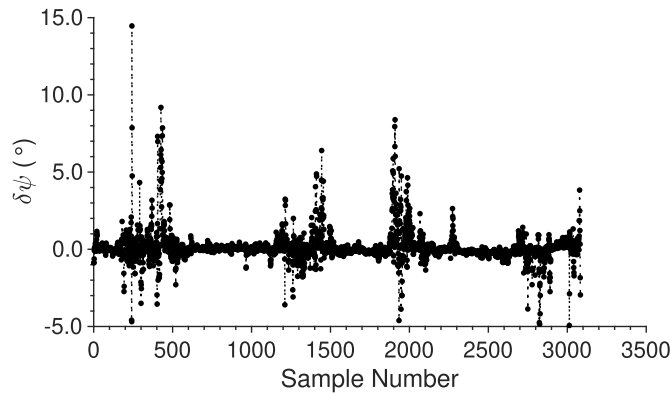


Fig. 10. Initial heading alignment errors by using STIM300 and NovAtel OEM6 GNSS receiver in typical urban environments.

To verify the application under urban environment, the proposed method was also tested in typical urban scenarios in Wuhan dense city areas, including boulevards, on viaducts, and between buildings. This field test used the same equipment as mentioned in Section IV-A. This experiment lasted about 2.5 h. The data can support 3083 alignment experiments with a 5-s alignment period, excluding GNSS-denied environments (e.g., tunnels) and low-speed situations.

Fig. 10 shows the heading errors of each independent sample based on STIM300 and NovAtel OEM6, in a typical urban scenario. We can notice that the heading errors of certain samples are significantly larger, and this is because the test contains some harsh scenarios, such as the GNSS signal just recovered (sample 242) or the vehicle turning (sample 1909), which cause serious deterioration of GNSS carrier phase. The result shows that even in a complex urban environment, the proposed method can reach the accuracy of 1.68° at a 95% confidence level with a 5-s alignment period. Fig. 11 shows the heading errors based on a low-cost GNSS receiver, i.e., u-blox M8P module in the same test as in Fig. 10. The result shows that in a complex urban environment, the proposed method with a low-cost GNSS receiver can reach the accuracy of 5.19° at a 95% confidence level with a 5-s alignment period.

Table II compares the statistical results for the tests above under different conditions and with different hardware configurations. The heading errors in open-sky environment are

TABLE II  
STATISTICS OF THE INITIAL HEADING ALIGNMENT ERRORS FOR DIFFERENT TEST CONFIGURATIONS

Test Configuration			Heading Error (°)		
Scenario	IMU	GNSS Receiver	CDF95	RMSE	Max
Open Sky	STIM300	NovAtel OEM6	0.65	0.27	1.66
	ICM20602	NovAtel OEM6	0.85	0.47	1.97
	STIM300	u-blox M8P	0.93	0.42	2.33
Urban	STIM300	NovAtel OEM6	1.68	0.96	14.46
	STIM300	u-blox M8P	5.19	3.65	53.49

obtained by averaging the results of all satellites, while the heading errors in complex urban environment only use the satellites with delta azimuth ranging from 30° to 150°. The accuracy decreased in the urban environment, especially when using a low-cost GNSS receiver module. The reasons for the decrease are most likely two aspects: 1) the GNSS signals are frequently reflected, blocked, and weakened in urban environments, which cause serious deterioration of GNSS carrier phase, and 2) the low-cost GNSS receivers do not perform well in the quality control of observations since the main goal of the low-cost GNSS receiver is to ensure the continuity of observations and positioning as much as possible.

D. Discussion

This article proposes a rapid and accurate heading initialization method using TDCP, achieving an accuracy of 0.65° with 95% confidence level within only 5 s under open-sky conditions, using high-performance MEMS IMU and high-quality GNSS receiver. One reason that the proposed method can achieve such accuracy is that the TDCP can provide accurate relative measurements with centimeter or even millimeter accuracy levels.

In this article, a straightforward approach by averaging is used to combine the heading results from multiple satellites to give the final initial heading. The accuracy of estimated heading is more reasonable when using a weight least squares (LS)

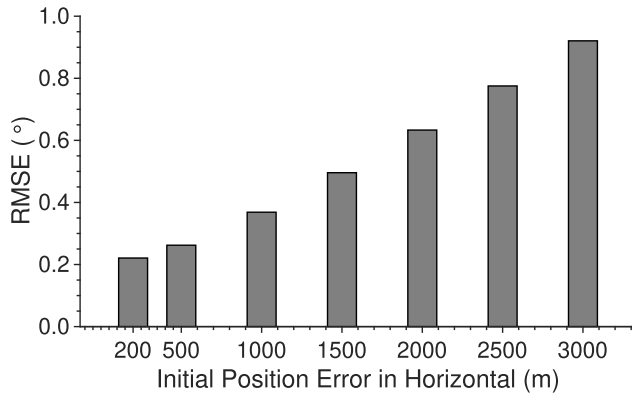


Fig. 12. RMSE of the initial heading with respect to initial position error.

or KF, especially in the urban environment. However, when there are a large number of high-quality observations, the advantage of using a weight LS or KF will not be that significant.

In theory, the proposed method can be used even under low satellite visibility. The experiment shown in this article was performed under open-sky area and used GNSS to provide the travel distance, which implies that at least four satellites are required. However, if an odometer is used instead of GNSS to provide the travel distance for the DR calculator, the proposed method can be performed with less than four satellites. Section II-C describes the calculation of the initial heading using the observations of only one satellite; however, there are two solutions of  $\alpha_u$  to function (28). This uncertainty can be eliminated by at least two satellites' solutions to function (28). Thus, the worst case where the method can be used is when only two satellites are visible. According to Fig. 7, the solution of an individual satellite generally achieves an accuracy of  $1.0^\circ$  at a 95% confidence level. This implies that the proposed method can rapidly and accurately obtain the initial heading even under low satellite visibility, which is significant in urban complex environments.

It should be noted that the proposed method is not sensitive to initial position errors, which is a requirement for the DR calculator. If an error exists in the initial position, under the condition that the error is not significantly large, for example, under 2 km, then we can consider that only a translational motion has occurred in the DR-derived trajectory when compared to error-free trajectory, which has a minimal effect on the azimuth of the trajectory. To verify the effect of the initial position error on heading alignment, Fig. 12 shows a plot of the RMSE of the alignment samples when an initial position error exists, using the dataset used in Fig. 4 whose RMSE is  $0.27^\circ$  when there is no initial position error. A certain position error disturbance (0.2–3 km) in the two orthogonal directions in the horizontal plane was separately added to the initial position. The corresponding alignment results were calculated and its RMSE was determined and plotted in Fig. 12. Fig. 12 shows that when the initial position error is 2 km, the RMSE value of the initial heading error is less than  $0.7^\circ$ , whereas the RMSE value of the initial heading error with no initial position error is  $0.27^\circ$ . In general,

an approximate initial position can be easily obtained for a vehicle as the last assembly position is usually saved locally in the vehicle. Thus, this method can be practically applied to vehicles, even under low satellite visibility.

## V. CONCLUSION

In this research, we proposed an initial heading alignment method for MEMS INS using the GNSS carrier-phase measurement based on the basic principle of trajectory similarity. The proposed method performed the trajectory matching in the LOS directions of satellites, where the angle is obtained by comparing the actual-observed TDCP and INS-derived TDCP. Experimental results showed that the proposed method can achieve an accuracy of  $0.65^\circ$  and  $1.68^\circ$  with a 95% confidence level in only 5 s under open-sky conditions and in typical urban environments, respectively, using a typical MEMS IMU and a high-quality geodetic GNSS receiver. Similar experiments using a low-cost IMU chip or a low-cost GNSS receiver module under different environments were also used to verify the proposed method. The results showed that this method exhibits considerable advantages in terms of rapidity, accuracy, and applicability when compared to existing alignment approaches.

## REFERENCES

- [1] Q. Chen, Q. Zhang, X. Niu, and J. Liu, "Semi-analytical assessment of the relative accuracy of the GNSS/INS in railway track irregularity measurements," *Satell. Navigat.*, vol. 2, no. 1, pp. 1–16, Dec. 2021.
- [2] Q. Zhang, S. Li, Z. Xu, and X. Niu, "Velocity-based optimization-based alignment (VBOBA) of low-end MEMS IMU/GNSS for low dynamic applications," *IEEE Sensors J.*, vol. 20, no. 10, pp. 5527–5539, May 2020.
- [3] S. Han and J. Wang, "A novel initial alignment scheme for low-cost INS aided by GPS for land vehicle applications," *J. Navigat.*, vol. 63, no. 4, pp. 663–680, Sep. 2010.
- [4] R. Sun, Q. Cheng, and J. Wang, "Precise vehicle dynamic heading and pitch angle estimation using time-differenced measurements from a single GNSS antenna," *GPS Solutions*, vol. 24, no. 3, pp. 1–9, Jul. 2020.
- [5] Y. Huang, Y. Zhang, and L. Chang, "A new fast in-motion coarse alignment method for GPS-aided low-cost SINS," *IEEE/ASME Trans. Mechatronics*, vol. 23, no. 3, pp. 1303–1313, Jun. 2018.
- [6] Y. Huang, Y. Zhang, and X. Wang, "Kalman-filtering-based in-motion coarse alignment for odometer-aided SINS," *IEEE Trans. Instrum. Meas.*, vol. 66, no. 12, pp. 3364–3377, Dec. 2017.
- [7] L. Chang, H. He, and F. Qin, "In-motion initial alignment for odometer-aided strapdown inertial navigation system based on attitude estimation," *IEEE Sensors J.*, vol. 17, no. 3, pp. 766–773, Feb. 2017.
- [8] L. Chang and B. Hu, "Robust initial attitude alignment for SINS/DVL," *IEEE/ASME Trans. Mechatronics*, vol. 23, no. 4, pp. 2016–2021, Aug. 2018.
- [9] X. Xu, Y. Sun, J. Gui, Y. Yao, and T. Zhang, "A fast robust in-motion alignment method for SINS with DVL aided," *IEEE Trans. Veh. Technol.*, vol. 69, no. 4, pp. 3816–3827, Feb. 2020.
- [10] Y. Wu, C. He, and G. Liu, "On inertial navigation and attitude initialization in polar areas," *Satell. Navigat.*, vol. 1, no. 1, pp. 1–6, Dec. 2020.
- [11] P. D. Groves, R. J. Handley, and S. T. Parker, "Vehicle heading determination using only single-antenna GPS and a single Gyro," in *Proc. 22nd Int. Tech. Meeting Satell. Division The Inst. Navigat. (ION GNSS)*, 2009, pp. 1775–1784.
- [12] Q. Chen, H. Lin, R. Guo, and X. Niu, "Rapid and accurate initial alignment of the low-cost MEMS IMU chip dedicated for tilted RTK receiver," *GPS Solutions*, vol. 24, no. 4, pp. 1–13, Oct. 2020.
- [13] P. Groves, *Principles of GNSS, Inertial, and Multisensor Integrated Navigation Systems*, 2nd ed. Norwood, MA, USA: Artech House, 2013.
- [14] D. Wang, H. Lv, and J. Wu, "In-flight initial alignment for small UAV MEMS-based navigation via adaptive unscented Kalman filtering approach," *Aerosp. Sci. Technol.*, vol. 61, pp. 73–84, Feb. 2017.

- [15] H. S. Hong, J. G. Lee, and C. G. Park, "Performance improvement of in-flight alignment for autonomous vehicle under large initial heading error," *IEE Proc.-Radar, Sonar Navigat.*, vol. 151, no. 1, pp. 57–62, Feb. 2004.
- [16] Y. Yang, H. He, and G. Xu, "Adaptively robust filtering for kinematic geodetic positioning," *J. Geodesy*, vol. 75, pp. 109–116, May 2001.
- [17] J. S. Li, J. N. Xu, L. B. Chang, and F. Zha, "An improved optimal method for initial alignment," *J. Navigat.*, vol. 67, no. 4, pp. 727–736, Jul. 2014.
- [18] P. M. G. Silson, "Coarse alignment of a ship's strapdown inertial attitude reference system using velocity loci," *IEEE Trans. Instrum. Meas. Soc.*, vol. 60, no. 6, pp. 1930–1941, Jun. 2011.
- [19] K. Taizhong, F. Jiancheng, and W. Wei, "In-flight calibration approach based on quaternion optimization for POS used in airborne remote sensing," *IEEE Trans. Instrum. Meas.*, vol. 62, no. 11, pp. 2882–2889, Nov. 2013.
- [20] L. Ma, K. Wang, and M. Shao, "Initial alignment on moving base using GPS measurements to construct new vectors," *Measurement*, vol. 46, no. 8, pp. 2405–2410, Oct. 2013.
- [21] M. Wu, Y. Wu, X. Hu, and D. Hu, "Optimization-based alignment for inertial navigation systems: Theory and algorithm," *Aerosp. Sci. Technol.*, vol. 15, no. 1, pp. 1–17, Jan./Feb. 2011.
- [22] E.-H. Shin and N. El-Sheimy, "An unscented Kalman filter for in-motion alignment of low-cost IMUs," in *Proc. PLANS Position Location Navigat. Symp.*, Apr. 2004, pp. 273–279.
- [23] Y. Wu and X. Pan, "Velocity/position integration formula—Part I: Application to in-flight coarse alignment," *IEEE Trans. Aerosp. Electron. Syst.*, vol. 49, no. 2, pp. 1006–1023, Apr. 2013.
- [24] L. Chang, J. Li, and K. Li, "Optimization-based alignment for strapdown inertial navigation system: Comparison and extension," *IEEE Trans. Aerosp. Electron. Syst.*, vol. 52, no. 4, pp. 1697–1713, Aug. 2016.
- [25] Y. Wei, H. Li, and M. Lu, "Carrier Doppler-based initial alignment for MEMS IMU/GNSS integrated system under low satellite visibility," *GPS Solutions*, vol. 25, no. 3, pp. 1–11, Jul. 2021.
- [26] S. de La Parra and J. Angel, "Low cost navigation system for UAV's," *Aerosp. Sci. Technol.*, vol. 9, no. 6, pp. 504–516, 2005.
- [27] F. Zangenehjad and Y. Gao, "GNSS smartphones positioning: Advances, challenges, opportunities, and future perspectives," *Satell. Navigat.*, vol. 2, no. 1, pp. 1–23, Dec. 2021.
- [28] R. M. Rogers, *Applied Mathematics in Integrated Navigation Systems* (AIAA Education Series), vol. 1. Washington, DC, USA: AIAA, 2003.
- [29] P. Savage, "Strapdown inertial navigation integration algorithm design—Part 1: Attitude algorithms," *J. Guid., Control Dyn.*, vol. 21, no. 1, pp. 19–28, Jan. 1998.
- [30] G. Xu and Y. Xu, *GPS: Theory, Algorithms and Applications*. Berlin, Germany: Springer, 2016.
- [31] P. G. Savage *et al.*, *Strapdown Analytics*, vol. 2. Maple Plain, MN, USA: Strapdown Associates Maple Plain, 2000.
- [32] G. Wang, X. Xu, J. Wang, and Y. Zhu, "An enhanced INS/GNSS tightly coupled navigation system using time-differenced carrier phase measurement," *IEEE Trans. Instrum. Meas.*, vol. 69, no. 7, pp. 5208–5218, Jul. 2020.
- [33] D. K. Elliott and J. Hegarty Christopher, *Understanding GPS: Principles and Applications*. Norwood, MA, USA: Artech house, 2006.
- [34] X. Niu, K. Yan, T. Zhang, Q. Zhang, H. Zhang, and J. Liu, "Quality evaluation of the pulse per second (PPS) signals from commercial GNSS receivers," *GPS Solutions*, vol. 19, no. 1, pp. 141–150, Jan. 2015.
- [35] W. Gao, X. Meng, C. Gao, S. Pan, Z. Zhu, and Y. Xia, "Analysis of the carrier-phase multipath in GNSS triple-frequency observation combinations," *Adv. Space Res.*, vol. 63, no. 9, pp. 2735–2744, May 2019.
- [36] H. Tang, X. Niu, T. Zhang, Y. Li, and J. Liu, "OdoNet: Untethered speed aiding for vehicle navigation without hardware wheeled odometer," *IEEE Sensors J.*, vol. 22, no. 12, pp. 12197–12208, Jun. 2022.



**Tisheng Zhang** received the B.Sc. and Ph.D. degrees in communication and information system from Wuhan University, Wuhan, China, in 2008 and 2013, respectively.

He held a post-doctoral position at The Hong Kong Polytechnic University, Hong Kong, from 2017 to 2018. He is currently an Associate Professor with the GNSS Research Center, Wuhan University. His research interests focus on the fields of global navigation satellite system (GNSS) receiver and multisensor integrated navigation.



**Shan Liu** received the B.E. degree in electronic information engineering from Wuhan University, Wuhan, China, in 2020, where she is currently pursuing the master's degree in navigation, guidance, and control with the GNSS Research Center.

Her primary research interests focus on deeply coupled global navigation satellite system (GNSS) receivers.



**Qijin Chen** received the B.Eng. and Ph.D. degrees in geodesy and survey engineering from Wuhan University, Wuhan, China, in 2011 and 2016, respectively.

He is currently an Associate Research Fellow with the GNSS Research Center, Wuhan University. His research interests include inertial navigation systems (INSs) with aiding and its applications in geodesy and precise surveying engineering, including railway track geometry measuring and underground pipeline surveying.



**Xin Feng** received the B.E. and M.E. degrees from Wuhan University, Wuhan, China, in 2018 and 2021, respectively, where he is currently pursuing the Ph.D. degree in geodesy and survey engineering with the School of Geodesy and Geomatics.

His primary research interests include global navigation satellite system (GNSS) receiver and multi-sensor ultratightly integrations.



**Xiaoji Niu** received the B.Eng. and Ph.D. degrees from the Department of Precision Instruments, Tsinghua University, Beijing, China, in 1997 and 2002, respectively.

He did his post-doctoral research at the University of Calgary, Calgary, AB, Canada. He was a Senior Scientist with SiRF Technology Inc., Shanghai, China. He is currently a Professor with the GNSS Research Center, Wuhan University, Wuhan, China. He has published more than 90 academic articles.

He leads the Multi-Sensor Navigation Group focusing on global navigation satellite system (GNSS)/inertial navigation system (INS) integrations, low-cost navigation sensor fusion, and its new applications.